

Calibrated and Partially Calibrated Semi-Generalized Homographies

Snehal Bhayani¹

Torsten Sattler²
Janne Heikkilä¹

Daniel Barath³
Zuzana Kukelova²

Patrik Beliansky⁴

¹Center for Machine Vision and Signal Analysis, University of Oulu, Finland

²Faculty of Electrical Engineering, Czech Technical University in Prague

³Computer Vision and Geometry group, ETH Zürich

⁴Faculty of Mathematics and Physics, Charles University, Prague

Abstract

In this paper, we propose the first minimal solutions for estimating the semi-generalized homography given a perspective and a generalized camera. The proposed solvers use five 2D-2D image point correspondences induced by a scene plane. One of them assumes the perspective camera to be fully calibrated, while the other solver estimates the unknown focal length together with the absolute pose parameters. This setup is particularly important in structure-from-motion and image-based localization pipelines, where a new camera is localized in each step with respect to a set of known cameras and 2D-3D correspondences might not be available. As a consequence of a clever parametrization and the elimination ideal method, our approach only needs to solve a univariate polynomial of degree five or three. The proposed solvers are stable and efficient as demonstrated by a number of synthetic and real-world experiments.

1 Introduction

The estimation of a homography between two cameras observing a planar scene is a crucial problem in computer vision with a number of applications, *e.g.*, in structure-from-motion (SfM) [42, 44, 46, 51], localization [6, 37, 39], visual odometry [31, 32], camera calibration [43, 52], and image retrieval [35, 50]. It is one of the oldest camera geometry problems with many so-

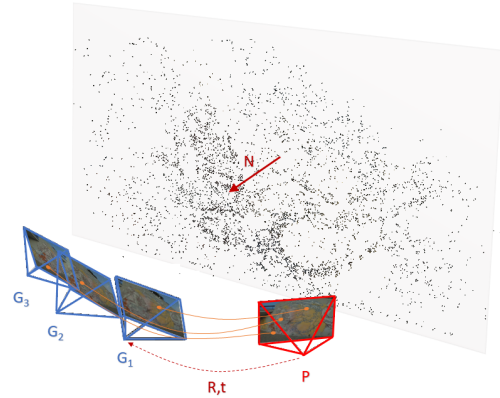


Figure 1: An illustration of the problem configuration.

lutions including the well-known normalized direct linear transform (DLT) method [17] for estimating the homography from a minimum of four point correspondences; the minimal solutions based on affine [3, 22] or SIFT correspondences [2, 4]; solutions assuming known gravity direction [13, 41]; or cameras with radial distortion [7, 9, 14, 17, 20, 25]. All above-mentioned algorithms assume that both cameras satisfy the central perspective projection model (potentially, with radial distortion), *i.e.*, they assume that both cameras have a single center of projection. Surprisingly, the problem of estimating a homography has not been studied for generalized cameras.

A generalized camera [36] is a camera that captures

some arbitrary set of rays and does not adhere to the central perspective projection model. Such a camera model is practical and appears, *e.g.*, in applications that exploit multi-camera configurations, like stereo-pairs or in localization pipelines [49]. Such pipelines often are based on sequences of images, where there might be a set of cameras with known poses and we are given a new image which is to be registered given the generalized camera, composed of the known perspective ones. Estimating the camera pose, *w.r.t.*, the generalized camera, in such situations often leads to results superior, in terms of accuracy, to considering only pair-wise epipolar geometries. Also, it has the advantage of recovering the absolute pose which is a severe deficiency of epipolar geometry-based relative pose estimation.

While the problem of estimating absolute pose of a generalized camera can be solved very efficiently [26], *i.e.*, there exist a solution that solves only 3 quadratic equations in 3 unknowns and runs in a few μs , the problem of estimating the relative pose of two generalized cameras is significantly more complex [45]. This problem results in a system of 15 polynomial equations, each of degree 6, with 64 solutions. The final solver based on the Gröbner basis method [45] is infeasible for real-time applications.

In [53], the authors considered a semi-generalized epipolar geometry problem, *i.e.*, the problem of estimating the relative pose together with the scale of the translation between one perspective and one generalized camera from 2D-2D correspondences. In this paper, 4 minimal solvers were presented, *i.e.*, E_{5+1} and E_{4+2} for calibrated pinhole cameras, and Ef_{6+1} and Ef_{5+2} for pinhole cameras with unknown focal length. The indices in the solver names denote the number of point correspondences coming from one camera G_i of the generalized camera G . The authors demonstrated the applicability of the proposed E_{4+2} and Ef_{5+2} solvers for incremental camera registration in the absence of 2D-3D point correspondences in an SfM pipeline. However, the E_{4+2} and Ef_{5+2} solvers perform operations on large matrices and, thus, are impractical for real-time applications, with running times of 1.2ms and 13.6ms, respectively. E_{5+1} and Ef_{6+1} solvers, also mentioned in this paper, are based on the existing efficient five-point $E5$ [33] and the six point $E6f$ [8] relative pose methods. These solvers actually do not bring any benefit from the generalized camera setup, except the fact that one additional point correspondence is

used for the estimation of the scale of translation. Moreover, the E_{5+1} and Ef_{6+1} solvers require 5 (6 for unknown focal length) point correspondences to be detected by the same camera. This criterion may be problematic in the absence of enough inliers point matches. Note that [53] does not solve all possible configurations of point correspondences that can appear in the semi-generalized setup due to the complicated systems of polynomial equations. The solvers proposed in [53] do not work if the generalized camera consists of more than two cameras and fewer than four correspondences come from a single camera.

In this paper, we study a similar camera setup as [53], *i.e.*, one perspective and one generalized camera. However, we assume that these cameras observe a planar scene, see Fig. 1. We present the first minimal solutions for estimating the pose between a perspective and a generalized camera from 2D-2D correspondences induced by a plane, *i.e.*, the first minimal solutions for the so-called *semi-generalized homography* problem. The proposed solvers use five 2D-2D image point correspondences and assume either a calibrated or a perspective camera with unknown focal length. This setup is particularly important in SfM and localization, where a new camera is localized with respect to a set of known ones and 2D-3D correspondences might not be available, *e.g.*, due to memory restrictions or to avoid matching features between individual cameras in the generalized camera.

The main **contributions** of the paper are as follows:

- A theoretical analysis of the **new semi-generalized homography** problem for calibrated and partially calibrated cameras with unknown focal length.
- Derivation of **new constraints** for the semi-generalized homography using the elimination ideal theory [27].
- **Four new efficient minimal solvers** $sh5_2$, $sh5_3$, $sh5f_2$ and $sh5f_3$, that only need to solve a univariate polynomial of degree five, respectively, three. Compared to existing ones, the new solvers do not need 3D points or 2D-2D correspondences between individual cameras from the generalized camera and cover all scenarios where it is possible to estimate the scale.
- Compared to [53], our solvers cover **all possible configurations of point correspondences** coming

from the generalized camera.¹

2 Problem Formulation

First, we set up notations and conventions that we will follow for the rest of the paper. Let P denote the perspective camera, while the generalized camera is denoted as G . We assume that the generalized camera G is fully calibrated, and it consists of a set of perspective cameras $\{G_1, G_2, \dots, G_k\}$. For the pinhole camera P , we consider two different cases, *i.e.*, the case where P is fully calibrated, and the case when its calibration matrix is of the form $K = \text{diag}(f, f, 1)$ with unknown focal length f .

In the following text, we will consider several different coordinate systems, *i.e.*, the global coordinate system, the local coordinate system of the perspective camera P , and local coordinate systems of perspective cameras G_i . Let R_{G_i} , t_{G_i} and R_P , t_P denote the rotations and translations required to align local the coordinate systems of G_i respectively P , to the global coordinate system. Without loss of generality, we can assume that the global coordinate system coincides with the local coordinate system of G_1 , *i.e.*, $R_{G_1} = I$ and $t_{G_1} = [0, 0, 0]^\top$. Sometimes we will call this system the local coordinate system of the generalized camera G . Therefore, the global coordinate system, the local coordinate system of G_1 , and the local coordinate system of G are interchangeable. We will use the upper index to denote the coordinate system. For example, $X^P \in \mathbb{R}^3$ and $X^G \in \mathbb{R}^3$ are the coordinates of the point X in the local coordinate system of P and the local coordinate system of G , respectively, and it holds that $X^G = R_P X^P + t_P$.

Our objective is to estimate the rotation $R \in \text{SO}(3)$ and translation $t \in \mathbb{R}^3$ between the perspective camera P and the generalized camera G , *i.e.*, the rotation and translation that align the local coordinate system of P to that of G . Note that since the local coordinate system of the generalized camera G coincides with the global coordinate

system, we have $R = R_P$ and $t = t_P$.

For the estimation of R and t , we will use 2D-2D correspondences detected between P and G_i . We assume, that these point correspondences are projections of co-planar 3D points X_j satisfying: $N^\top X_j + d = 0$, where N denotes the normal of the scene plane π and d denotes the plane intercept. Note that the same plane can be defined by the normal $\tilde{N} = N/d$ and the equation $\tilde{N}^\top X_j + 1 = 0$.

2.1 Semi-Generalized Homography

Let us assume a 3D point X_j observed by the perspective camera P and the camera G_i , *i.e.*, the i -th constituent perspective camera from the generalized camera G . Let us denote the image points detected in P and G_i as $p_j = [x_j, y_j, 1]^\top$ and $g_{ij} = [x_j^{G_i}, y_j^{G_i}, 1]^\top$, respectively. With this notation, the coordinates of the 3D point X_j in the local coordinate system of P can be expressed as

$$X_j^P = \alpha_j K^{-1} p_j, \quad (1)$$

where K is the calibration matrix of the camera P and α_j represents the depth of the point X_j in P . A similar relationship holds for the coordinates of the 3D point X_j in the local coordinate system of G_i ,

$$X_j^{G_i} = \beta_{ij} K_{G_i}^{-1} g_{ij}, \quad (2)$$

where K_{G_i} is the calibration matrix of the camera G_i and β_{ij} represents the depth of the point X_j in G_i .

To obtain the relationship between X_j^P and $X_j^{G_i}$ we have to transform them into the same coordinate system, *i.e.*, in this case the global coordinate system. This gives us the following constraint

$$\alpha_j R K^{-1} p_j + t = \beta_{ij} R_{G_i} K_{G_i}^{-1} g_{ij} + t_{G_i}. \quad (3)$$

Note, that here we use the fact that $R = R_P$ and $t = t_P$. Since, in our case R_{G_i} , t_{G_i} and $K_{G_i}^{-1}$ are known, we will, for better readability, substitute $q_{ij} = R_{G_i} K_{G_i}^{-1} g_{ij}$ and obtain

$$\alpha_j R K^{-1} p_j + t = \beta_{ij} q_{ij} + t_{G_i}. \quad (4)$$

The 3D points X_j lying on the plane π , *i.e.*, X_j^P should satisfy $(\tilde{N}^P)^\top X_j^P + 1 = 0$, where $\tilde{N}^P \in \mathbb{R}^3$ is the normal of the plane π in the local coordinate system of P . For simplicity, in the rest of the text, we will omit the upper

¹For the case where the perspective camera P is calibrated the problem of homography estimation when four point correspondences are coming from the same camera G_i in the generalized camera G , can be considered as a problem of homography estimation from these four point correspondences [17] while the fifth point correspondence can be used to estimate the scale of the translation. However for the case when the focal length of P is unknown, it can be proved that the scale of translation can not be recovered.

index P in $\tilde{\mathbf{N}}^P$. The depth α_j in (1) can be then expressed using the normal $\tilde{\mathbf{N}}$ as

$$\alpha_j = \frac{-1}{\tilde{\mathbf{N}}^\top \mathbf{K}^{-1} \mathbf{p}_j}. \quad (5)$$

Let us consider a 3×3 homography matrix \mathbf{H} of the form $\mathbf{H} = \mathbf{R} - \mathbf{t}\tilde{\mathbf{N}}^\top$. By substituting (5) into (4) we obtain

$$\alpha_j \mathbf{H} \mathbf{K}^{-1} \mathbf{p}_j = \beta_{ij} \mathbf{q}_{ij} + \mathbf{t}_{G_i}. \quad (6)$$

We call this equation the semi-generalized homography constraint.

The depths β_{ij} can be easily eliminated from (6) by multiplying it with the skew-symmetric matrix $[\mathbf{q}_i]_\times$ from the left side, resulting in

$$[\mathbf{q}_{ij}]_\times (\alpha_j \mathbf{H} \mathbf{K}^{-1} \mathbf{p}_j - \mathbf{t}_{G_i}) = 0. \quad (7)$$

Let us denote $\mathbf{G} = \mathbf{H} \mathbf{K}^{-1}$. By dividing (7) with α_j and using (5), we obtain the equation

$$[\mathbf{q}_{ij}]_\times (\mathbf{G} \mathbf{p}_j + (\mathbf{M}^\top \mathbf{p}_j) \mathbf{t}_{G_i}) = 0, \quad (8)$$

where $\mathbf{M} = \mathbf{K}^{-1} \tilde{\mathbf{N}}$. Note that this special parameterization, based on the normal of the plane expressed in the coordinate system of P , allowed us to eliminate the unknown depths α_j from (7), and to derive linear constraints for the semi-generalized homography. Each 2D-2D correspondence $\mathbf{p}_j \leftrightarrow \mathbf{q}_{ij}$ gives us three equations of the form (8) from which only two are linearly independent.

2.2 Semi-generalized Homography Constraints

Besides the constraints (8) induced by a 2D-2D correspondence $\mathbf{p}_j \leftrightarrow \mathbf{q}_{ij}$, there are other ones arising from the form of the matrix \mathbf{G} . The constraints (8) are linear in the 12 unknowns, *i.e.*, elements of the matrix \mathbf{G} and the vector \mathbf{M} . However, \mathbf{G} and \mathbf{M} are not independent since $\mathbf{G} = \mathbf{H} \mathbf{K}^{-1} = \mathbf{R} \mathbf{K}^{-1} - \mathbf{t} \mathbf{M}^\top$. Moreover, the rotation matrix $\mathbf{R} \in \mathbf{SO}(3)$ introduces additional constraints. All these constraints, *i.e.*, constraints originating from the form

$$\mathbf{G} - \mathbf{R} \mathbf{K}^{-1} + \mathbf{t} \mathbf{M}^\top = 0, \quad \mathbf{R}^\top \mathbf{R} = \mathbf{R} \mathbf{R}^\top = \mathbf{I}_{3 \times 3}, \quad (9)$$

can be used to define an ideal $I \subset \mathbb{C}[\varepsilon]$ [12], where ε contains 9 unknowns from \mathbf{G} , 9 from \mathbf{R} , 3 from \mathbf{t} , 3 from

\mathbf{M} and the inverse of the focal length $w = \frac{1}{f}$. Now we can use the elimination ideal technique [27] to eliminate 9 unknowns of \mathbf{R} , 3 of \mathbf{t} , and w from this ideal. *I.e.*, we compute an elimination ideal I_1 that will contain only polynomials in 12 unknowns from \mathbf{G} and \mathbf{M} . Note, that this elimination ideal can be computed offline using some algebraic geometry software like Macaulay 2 [16]. We found that such an elimination ideal is generated by 4 polynomials (3 of degree 3 and 1 of degree 4) in 12 unknowns. Similarly, for the calibrated case, *i.e.*, $\mathbf{K} = \mathbf{I}$ there are 10 such generators of I_1 . For more details on elimination ideals we refer to [12, 27].

These 4 new constraints (10 for the calibrated case) in 12 unknowns from \mathbf{G} and \mathbf{M} together with the linear equations (8) in these unknowns can be used to solve our problem. After a null-space re-parameterization of \mathbf{G} and \mathbf{M} using the linear equations, we can transform these equations to 4 (10) polynomial equations in 2 unknowns. Such systems can be solved, *e.g.*, using the automatic generator of Gröbner basis solvers [23, 29]. This results in performing Gauss-Jordan (G-J) elimination of a 12×28 matrix and Eigenvalue decomposition of a 16×16 matrix for the calibrated case and G-J elimination of a 6×12 matrix and Eigenvalue decomposition of a 6×6 matrix for the unknown focal length case. The solvers return up to 16 (calibrated), respectively 6 (unknown f), real solutions to \mathbf{G} and \mathbf{M} .

However, in our case we want to make the solver as efficient as possible. Therefore, we introduce an additional change of variables by assuming that one of the elements of \mathbf{G} is non-zero, *e.g.*, $g_{33} \neq 0$. This assumption introduces a degeneracy. However, such a degeneracy is not crucial in practical applications and can be avoided, as it was discussed in [11]. Moreover, our change of coordinate system used for the calibrated solver directly avoids this degeneracy. The situation for the focal length case is discussed in more detail in the supplementary material.

With this assumption, we introduce new variables $g'_{kl} = \frac{g_{kl}}{g_{33}}$, for $\forall kl \neq 33$ and $m'_k = \frac{m_k}{g_{33}}$, $k = 1, \dots, 3$, where g_{kl} are elements from the k^{th} row and l^{th} column of matrix \mathbf{G} and m_k are elements of the vector \mathbf{M} . This variable change is also applied to the four generators of I_1 , defining a new ideal I'_1 . Using the same elimination ideal technique [27] that we used for obtaining generators of I_1 , we can eliminate g_{33} from the ideal I'_1 , leading to a

new ideal I'_2 , which is generated by only a single polynomial f of degree five in 8+3 unknowns g'_{kl} for $\forall kl \neq 33$ and m'_k , $k = 1, 2, 3$. For the calibrated case, the ideal I'_2 so obtained is generated by five polynomials, each of degree five, and in the 8+3 unknowns, g'_{kl} for $\forall kl \neq 33$ and m'_k , $k = 1, 2, 3$. More details on the form of the generators of the elimination ideals I_1 and I'_2 for both the cases, together with the input code for Macaulay2 used to compute these generators is provided in the supplementary material.

Note that the derivation of this 5th degree constraint f as well as the above mentioned generators of I_1 is crucial for the efficiency of the final solvers. Without using the elimination ideal tricks, one would need to work directly with the parameterization of G using the rotation matrix, leading to complex systems of polynomial equations in many unknowns and with huge solvers. Next, we show how to solve these equations for a P with the unknown focal length, as well as for a calibrated P .

2.3 Unknown Focal Length Solvers

In the case of unknown focal length, the calibration matrix of P has the form $K = \text{diag}(f, f, 1)$ and we have 10 DOF, 3 for each of R , t and \tilde{N} , and 1 for f . Therefore, we need five 2D-2D correspondences $\mathbf{p}_j \leftrightarrow \mathbf{q}_{ij}$, $j = 1, \dots, 5$, to solve this problem. Without loss of generality, we can assume that the first point correspondence is observed in camera G_1 , i.e., $i = 1$. For $i = 1$, we have $\mathbf{t}_{G_1} = [0, 0, 0]^T$. Moreover, without loss of generality we can pre-rotate the local coordinate systems of P and G_1 such that $\mathbf{p}_1 = [1, 0, 1]^T$ and $\mathbf{q}_{11} = [0, 0, 1]^T$. This simplifies the equations, and after substituting into (8), gives

$$g_{13} = -g_{11}, \quad g_{23} = -g_{21}. \quad (10)$$

The remaining four 2D-2D correspondences give us 8 linearly independent constraints of the form (8). Note, that (8) are homogeneous in the elements of G and M . Therefore, assuming $g_{33} \neq 0$, we can divide those equations with g_{33} . This, together with (10), transforms the equations (8) into non-homogeneous equations in 9 unknowns, i.e., $\varepsilon' = \{g'_{11}, g'_{12}, g'_{21}, g'_{22}, g'_{31}, g'_{32}, m'_1, m'_2, m'_3\}$. We can rewrite these equations in a matrix form as follows:

$$\mathbf{C}\mathbf{b} = 0, \quad (11)$$

where \mathbf{C} is a 8×10 coefficient matrix and \mathbf{b} is a 10×1 vectorized form of the set of $\varepsilon' \cup \{1\}$. Next, we consider two different situations based on the maximum number of correspondences coming from one camera G_i .

sH5f₂ solver: Assuming that no more than 2 correspondences are coming from the same camera G_i , the matrix \mathbf{C} in (11) has a two dimensional null-space $\{\mathbf{b}_1, \mathbf{b}_2\}$. A solution to \mathbf{b} can be obtained as a linear combination $\mathbf{b} = \gamma_1 \mathbf{b}_1 + \gamma_2 \mathbf{b}_2$. From the constraint $b_{10} = 1$, we can express γ_2 as a linear polynomial in γ_1 . Hence the variables in ε' can be parameterized as linear polynomials of γ_1 . Substituting such parameterization into the generator f of the ideal I'_2 described in the previous section yields a univariate polynomial $f(\gamma_1)$ of degree five. This polynomial can be efficiently solved using Sturm sequences [19].

The next step is to extract solutions to g_{33} and f . Writing $G = (RK^{-1} - tM^T)$, we obtain a set of polynomial constraints. By variable elimination and substitutions, we obtain 2 solutions to g_{33} , unique up to a sign, which is fixed by constraining the solution of the plane vector \mathbf{N} so that the corresponding 3D point in P is in the front of the camera. Moreover, using a similar approach we obtain a unique solution to the focal length f . Solutions to G as well as M can be extracted from the solutions to ε' and g_{33} . Knowing f , we can compute $H = GK$ as well as $N = KM$. Decomposing the homography matrix H leads to set of relative poses, R and t , from which we choose the feasible poses.

sH5f₃ solver: If there are three 2D-2D point correspondences coming from the same camera G_i , the situation is a bit different. Let us assume, without loss of generality, that the points \mathbf{q}_{i2} and \mathbf{q}_{i3} are observed in camera G_1 , i.e., $i = 1$. This is the same camera that observed the point \mathbf{q}_{11} . The remaining two points can be observed by one camera $G_j \neq G_1$ or by two different cameras $G_j \neq G_k \neq G_1$. In this case, G-J elimination of the matrix \mathbf{C} in (11) leads to a matrix of a special form

$$\begin{bmatrix} \mathbf{I}_{6 \times 6} & \mathbf{0}_{6 \times 6} & \mathbf{0}_{6 \times 1} & \mathbf{c}_{6 \times 1} \\ \mathbf{0}_{2 \times 6} & \mathbf{I}_{2 \times 2} & \mathbf{d}_{2 \times 1} & \mathbf{e}_{2 \times 1} \end{bmatrix} \mathbf{b} = \mathbf{0}, \quad (12)$$

where the indices in matrices and vectors indicate their sizes. Since $\mathbf{b} = [g'_{11}, g'_{12}, g'_{21}, g'_{22}, g'_{31}, g'_{32}, m'_1, m'_2, m'_3, 1]^T$, the first six rows of (12) give us directly a solution to g'_{kl} . The last

two rows can be used to express m'_1, m'_2 as a linear function of m'_3 . Substituting these expressions for m'_1, m'_2 and the extracted solution to g'_{kl} into the polynomial f gives us a univariate polynomial in m'_3 of degree 3. The remaining steps are similar to the $sHf5_2$ solver.

2.4 Calibrated Camera Solvers

We approach the case of a calibrated pinhole camera P in a similar way as the unknown focal length case. In this case, we can assume that $K = I_{3 \times 3}$ and therefore $G = H = R - t\tilde{N}^\top$. Here, we have 9 DOF, 3 for each R , t and \tilde{N} and 4.5 correspondences are sufficient to solve this problem. In practice, we still need to sample 5 points and we can use one constraint to eliminate geometrically infeasible solutions.

For the calibrated case, without loss of generality, we can assume that the first point correspondence was observed in camera G_1 , *i.e.*, $i = 1$ where $t_{G_1} = [0, 0, 0]^\top$, and pre-rotate the local coordinate systems of P and G_1 such that $p_1 = [0, 0, 1]^\top$ and $q_{11} = [0, 0, 1]^\top$. This simplifies the equations and, after substituting into (8), we have $g_{13} = 0$, $g_{23} = 0$. Similar to the case of unknown focal length, we have 8 homogeneous linearly independent constraints of the form (8) from the remaining 4 correspondences. In this case, we can safely assume $g_{33} \neq 0$ and divide these equations by g_{33} , transforming them into non-homogeneous equations in 9 unknowns, ε' . Based on the number of point correspondences coming from the same camera, G_i , we again consider two different solvers. Their formulations differ only in our approach for estimating solutions to variables in ε' , while the remaining steps are the same as for $sHf5_2$ solver in Section 2.3.

sH5₂ solver: This case is analogous to that of the $sH5f_2$ solver, where we have no more than 2 correspondences coming from the same camera G_i . Thus, the variables in ε' , following the approach used for $sHf5_2$, can be expressed as linear polynomials in one variable γ . This parameterization can be substituted into the generators of the ideal I'_2 for the calibrated case. Here, it leads to 5 univariate polynomials, each of degree 5. Without loss of generality, we can choose one of these polynomials, which we solve using Sturm sequences. This results in up to five real solutions to ε' .

sH5₃ solver: When we have three 2D-2D point correspondences coming from the same camera G_i , we have an analogous case to that of the $sHf5_3$ solver. Here, similar to the $sHf5_3$ solver, we can express m'_1, m'_2 as a linear function of m'_3 and compute g'_{kl} directly from the matrix of the form (12). Substituting this parameterization into the generators of I'_2 yields five univariate polynomials, each of degree three. We can obtain up to three real solutions to ε' by solving one of these polynomials using Sturm sequences [19].

3 Experiments

In this section, we study the performance of the proposed $sH5_2$, $sH5_3$, $sH5f_2$ and $sH5f_3$ solvers both on synthetic and real-world images. For comparison, we use four state-of-the-art minimal solvers for estimating the semi-generalized epipolar geometry [53], *i.e.*, the E_{5+1} , E_{4+2} , $E_{f_{6+1}}$ and $E_{f_{5+2}}$ solvers. Note, that for the experiments where we do not need the scale of the translation, E_{5+1} reduces to the well-known 5pt solver $E5$ [33] and the $E_{f_{6+1}}$ problem reduces to the one-sided focal length 6pt solver $E6f$ [8]. In such experiments we also consider the 4pt homography solver $H4$ [18]. We excluded the $E_{f_{5+2}}$ solver from real experiments since it was too slow when used on large datasets inside RANSAC. For a fair comparison, we further consider $P3P/P5Pf + N$ solvers. We designed these solvers for this particular semi-generalized homography setup. To the best of our knowledge such solvers have not been considered in the literature before. In these solvers, we first use three correspondences between two calibrated generalized cameras G_i and G_j to estimate the normal N and intercept d of the observed plane π . This information is then used to transform 3/5 2D-2D correspondences between the perspective camera P and arbitrary cameras in the generalized camera G to 2D-3D correspondences. Finally, the pose of the perspective camera is computed using the well-known $P3P$ [34] or $P5Pf$ [24] solvers. In the unknown focal length case, we use the non-minimal $P5Pf$ solver since the available implementations of the minimal $P4Pf$ one were either much slower than the $P5Pf$ solver or did not work for planar scenes. Note that these $P3P/P5Pf + N$ solvers, compared to the proposed solvers, require point correspondences between two cameras G_i and G_j in the generalized camera. However, these

correspondences are used only in the first step, when estimating the normal and plane intercept. Therefore, they do not need to be visible in camera P as in the standard 2D-3D pipeline.

3.1 Synthetic Scenes

We studied the performance of our proposed solvers on synthetically generated 3D scenes with known ground truth parameters. The 3D points were randomly distributed on a plane of size 10×10 . Each 3D point was projected into up to six cameras with realistic focal lengths. Five of these cameras represent the generalized camera G and one camera is considered as the camera P . The orientations and positions of the cameras were selected at random such that they look towards the origin from a random distance, varying from 20 to 35, from the plane. The simulated images have a resolution of 1000×1000 px. Here, we study the errors in the estimated rotations R for the calibrated solvers as well as the unknown focal length solvers. The plots for the pose and focal length error are, due to the lack of space, in the supplementary material. The rotation error is computed as the angle in the axis angle representation of $R_{GT}^{-1}R$, where R_{GT} is the ground truth while R is the estimated rotation.

Numerical stability. In order to study the numerical stability of the proposed solvers, we evaluated 5K camera setups for planar scenes. We compare the accuracy of the rotations estimated by the proposed solvers $sH5_3$ and $sH5_2$ with that of E_{5+1} , E_{4+2} and $P3P + N$ in Fig. 2(a). The proposed solvers achieve comparable stability with fewer failures (*i.e.*, no peak on the right side) as compared to the other solvers. Similarly, Fig. 2(e) provides a comparison of the numerical stability of the proposed $sH5f_3$ and $sH5f_2$ with that of the solvers Ef_{6+1} , Ef_{5+2} and $P5Pf + N$. The proposed solvers achieve state-of-the-art stability. We also note that the stability experiments being conducted on planar scenes created a degenerate configuration for the Ef_{6+1} solver which explains the reported performance.

Image noise. Next, we tested the performance of all solvers in the presence of Gaussian noise with standard deviation σ , added to the image points in all cameras. Fig. 2(b,f) show the rotation error (in degrees) for solvers for calibrated as well as partially calibrated cameras.

Here, we depict the results using the MATLAB function `boxplot` which shows 25% to 75% quantile values as boxes with a horizontal line for median. We note that our proposed solvers $sH5_2$ and $sH5f_2$ has comparable performance to the competitive solvers in the presence of image noise.

Close-to-planar scenes. We also considered the case where the scene is close to being entirely planar by having the scene plane at $z = 0$ and sampling 3D points with varying plane-to-point distance. Figures 2(c,g) show the errors in the estimated rotations for solvers assuming calibrated (c) or partially calibrated (g) cameras. The proposed solvers $sH5_2$ and $sH5f_2$ are more accurate or comparable to solvers $P3P + N$ and $P5Pf + N$ for close-to-planar scenes. It is clear that the quality of the estimates obtained using the proposed solvers deteriorates with the increasing non-planarity of the scene. However, the errors, even for larger non-planarity, correspond to the errors obtained by all competitive general solvers in the presence of 2 px image noise.

Forward motion with image noise. Next experiment evaluates the performance of the solvers for a forward moving camera in the presence of image noise. Figures 2(d,h) show the ground-truth error in the estimated rotation by the solvers for calibrated as well as partially calibrated cameras. Our proposed solver for calibrated cameras has comparatively better stability than the competing solvers. In case of unknown focal length solvers, we note that our proposed solvers lead to reasonable estimates to rotation. We note that in case of a pure forward motion, the solver Ef_{5+2} either failed or led to very unstable results. As a result of this, we have not considered the solver Ef_{5+2} in the graphs.

3.2 Computational Complexity

We report the computational complexity of the studied solvers in Tab. 1. Since we do not have an equally efficient C++ implementations of all solvers (some solvers are highly optimized, *e.g.*, $E5$ and $P3P$ from the PoseLib [28] library, while some do not contain any special optimization, *e.g.*, E_{4+2} , Ef_{5+2} [53]), we compare only the most time consuming operations performed by these solvers. For this we consider the matrix size for each of the critical

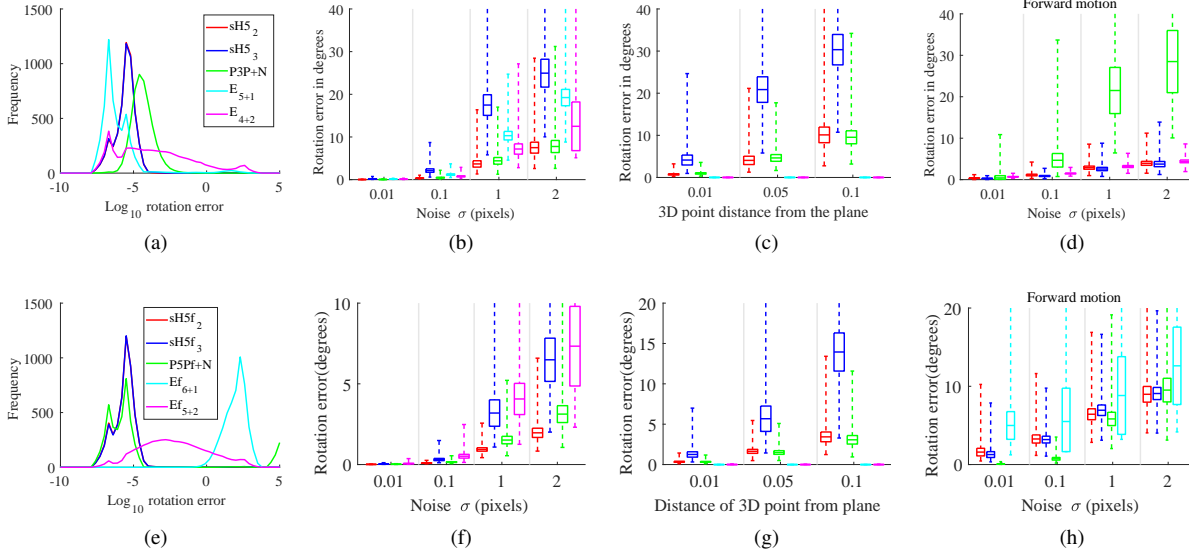


Figure 2: **Top:** Solvers for calibrated cameras, **Bottom:** Solvers for partially calibrated cameras: (a,e) Numerical stability. (b,f) Performance in the presence of image noise. (c,g) Close-to-planar scenes. (d,h) Forward motion in the presence of image noise.

	E_{5+1}	E_{4+2}	Ef_{6+1}	Ef_{5+2}	P3P+N	P5Pf+N	sH5 ₂	sH5 ₃	sH5f ₂	sH5f ₃
Reference	[53]	[53]	[53]	[53]						
Focal length			✓	✓		✓			✓	✓
# points	6	6	7	7	6	8	5	5	5	5
# solutions	10	40	10	50	4	4	5	3	5	3
Complexity										
G-J	10×20	73×113	11×20	378×428		5×8	8×10	8×10	8×10	8×10
Eigen		40×40	9×9	50×50	3×3					
Sturm	10						5	3	5	3
QR	9×5					8×5				

Table 1: Comparison of the proposed solvers (gray) vs. the state-of-the-art.

matrix operations, *e.g.*, 4×8 for G-J operation denotes a Gauss-Jordan elimination of a matrix of size 4×8 .

3.3 Real-World Experiments

In the proposed solvers, we built on the fact that man-made environments frequently contain planes and planar structures both indoor and outdoor. However, to demon-

strate their applicability in practice, we tested the solvers on general real-world data. Our objective is to show the usefulness of the proposed solvers in real applications like visual odometry and localization. Such general scenarios will of course give an advantage to our competitors, *e.g.*, [33], that work for planar as well as non-planar scenes. However, we will show that our new proposed

Method	King's	Old	Shop	St. Mary
sH5 ₃ (top-2) (ours)	0.58/0.76	2.16/3.88	0.14/0.60	1.19/3.46
E ₄₊₂ [54] (top-2)	1.25/1.91	2.33/3.72	0.19/0.79	1.07/2.45
E ₅₊₁ [54] (top-2)	0.41/0.59	1.07/2.28	0.11/0.42	0.27/0.80
sH5 ₂ & sH5 ₃ (top-10)	0.24/0.42	0.85/3.29	0.07/0.31	0.44/1.67
Sift+5Pt [55]	0.48/1.13	0.88/ 1.91	0.17/0.99	0.35/1.58

Table 2: Localization results on the Cambridge Landmarks dataset [21]. We report the median position (in meters) and rotation (in degrees) errors. For Sift+5Pt, we report the detailed results from [56] instead of the aggregated results from [55].

solvers return comparable pose and focal length estimates and sometimes even outperform the state-of-the-art general solvers for estimating the epipolar geometry or absolute pose. As such, we believe that our solvers can be combined with existing ones in a hybrid RANSAC [10], where the most suitable solver is selected for each scene in a data-dependent manner.

Localization Experiment. In this experiment, we evaluate the performance of our sH5₂ and sH5₃ solvers for calibrated cameras in the context of visual localization. We use the King’s College, Old Hospital, Shop Facade, and St. Mary’s Church scenes from the Cambridge Landmarks dataset [21] commonly used in the literature [40]. We report the median position and orientation error for each method.

The solvers sH5₂, sH5₃, E₄₊₂, and E₅₊₁ enable a particularly light-weight type of structure-less localization pipelines that do not need to store a 3D model, resulting in a representation that can be easily maintained [48]. In contrast to P3P + N and the SfM-on-the-fly approach from [48], they only require matches between the pinhole image and the generalized camera images, but not within images in the generalized camera, thus keeping feature matching to a minimum. We implement such a pipeline by using DenseVLAD-based image retrieval [47] to identify the top- k reference images most similar to a given query. The generalized camera is then defined using the known poses of the top- k retrieved images. The E₄₊₂ and E₅₊₁ solvers require matches to come from two cameras in a generalized camera. Thus, we use only the top-2 retrieved images. For a fair comparison, we compare against using sH5₃ for the top-2 retrieved images. Both

sH5₃ and sH5₂ can handle more images and we use the top-10 retrieved images to demonstrate the advantages of this property. In this case, we adaptively choose between sH5₂ and sH5₃ inside RANSAC, selecting the solver that is applicable for a given sample. All methods are integrated into LO-RANSAC [30, 38]. See the supp. material for details.

Tab. 2 shows the results of our experiments. As can be seen, our sH5₃ solver outperforms the E₄₊₂ solver but not the E₅₊₁ solver. However, using more images to define the generalized cameras, as afforded by the sH5₂ solver, can lead to a significant improvement in most scenes. The fact that E₅₊₁ still performs better on St. Mary’s Church can be attributed to the fact that this scene contains multiple parts without large planar structures. Combining our solvers with E₅₊₁ inside a hybrid RANSAC scheme should deliver the best from both types of solvers.

For comparison, Tab. 2 also includes the method from [55], which estimates the relative pose between the query and retrieved images based on SIFT feature matches and essential matrix estimation. The relative poses, with unknown scale of translation, are then used to triangulate the query pose using the known poses of the retrieved images. Our approach outperforms [55] on most scenes.

Relative Pose Experiments. The KITTI benchmark [15] consists of 22 stereo sequences captured by two front-facing cameras mounted to a moving vehicle. Out of the 22, only 11 sequences (00–10) provide the ground truth trajectories. We therefore used these 11 sequences (23,190 image pairs in total) to evaluate the compared solvers. In each scene, we considered the moving camera pair as the generalized camera and estimated the relative pose between the current camera pair and the left image of the next frame.

For testing the minimal solvers on real-world data, we chose a locally optimized RANSAC [30], *i.e.*, GC-RANSAC [5]. In GC-RANSAC, two different solvers are used: (a) one for estimating the pose from a minimal sample and (b) one for fitting to a larger-than-minimal sample when polishing the model parameters on a set of inliers. We included the compared solvers in step (a). For step (b), we applied a numerical optimization (implemented in the Ceres library [1]), minimizing the Sampson distance when estimating the essential matrix, and the re-

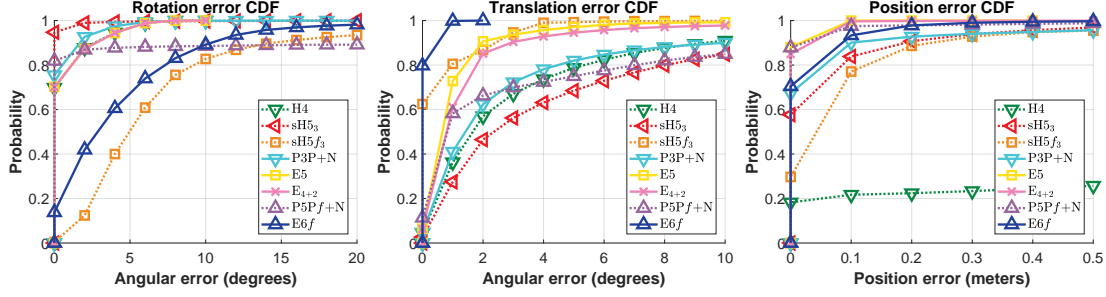


Figure 3: The cumulative distributions functions of the rotation, translation (both in degrees) and position (in meters) errors on the 23,190 image pairs from the KITTI dataset. A method being accurate is interpreted as a curve close to the top-left corner. Since most tested methods do not return the magnitude of the translation due to estimating the relative pose, we used the scale from the ground truth path to calculate the position error.

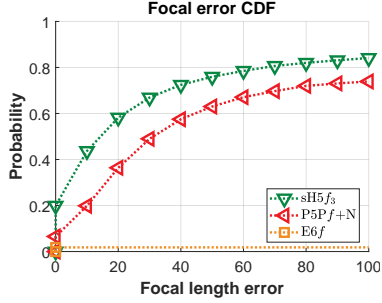


Figure 4: The cum. distributions functions of the focal length errors on the 23,190 image pairs from the KITTI dataset. A method being accurate is interpreted as a curve close to the top-left corner.

projection error when estimating the homography.

The cumulative distribution functions of the rotation, translation (both in degrees) and position (in meters) errors on the 23,190 image pairs from the KITTI dataset are shown in Fig. 3. Since some of the tested methods, *e.g.*, E5, do not return the magnitude of the translation due to estimating the relative pose, we used the scale from the ground truth path to calculate the position error. It can be seen that the proposed $sH5f_3$ solver leads to the most accurate rotations. The proposed $sH5f_3$ solver is amongst the top-performing methods in terms of translation error. The focal length errors for the proposed $sH5f_3$ and the $P5Pf+N$ and $E6f$ methods are shown in Fig. 4. As it is well-known [24], the $E6f$ solvers does not

provide a reasonable focal length when the cameras undergo forward motion, which is often the case when having vehicle-mounted cameras. The proposed $sH5f_3$ solver estimates significantly more accurate focal lengths than the $P5Pf+N$ solver.

4 Conclusion

In this paper, we have considered the problem of estimating the semi-generalized homography between a pinhole and a generalized camera. We have proposed efficient solvers handling for both calibrated pinhole cameras and partially calibrated pinhole cameras with unknown focal length. Our solvers cover all possible combinations of point correspondences between the pinhole and the generalized camera. To the best of our knowledge, we are the first to solve this problem. Through synthetic experiments and real experiments focusing on two real-world applications (localization and relative pose estimation for self-driving cars), we have shown that our proposed solvers are of practical relevance. While they may not be able to outperform more general existing solvers, which handle non-planar scenes, under all conditions, our results show that our solvers are preferable in certain conditions. Combining all these types of solvers into a single hybrid RANSAC approach is thus an interesting direction for future work.

References

- [1] Sameer Agarwal, Keir Mierle, and Others. Ceres solver. <http://ceres-solver.org>. 9
- [2] Daniel Barath. Five-point fundamental matrix estimation for uncalibrated cameras. In *Proceedings of the IEEE Conference on Computer Vision and Pattern Recognition*, pages 235–243, 2018. 1
- [3] Daniel Barath and Levente Hajder. A theory of point-wise homography estimation. *Pattern Recognition Letters*, 94:7–14, 2017. 1
- [4] Daniel Barath and Zuzana Kukelova. Homography from two orientation-and scale-covariant features. In *Proceedings of the IEEE International Conference on Computer Vision*, pages 1091–1099, 2019. 1
- [5] Daniel Barath and Jiří Matas. Graph-cut RANSAC. In *Computer Vision and Pattern Recognition (CVPR)*, 2018. 9
- [6] Eric Brachmann and Carsten Rother. Expert sample consensus applied to camera re-localization. In *ICCV*, 2019. 1
- [7] Matthew Brown, Richard I Hartley, and David Nistér. Minimal solutions for panoramic stitching. In *2007 IEEE Conference on Computer Vision and Pattern Recognition*, pages 1–8. IEEE, 2007. 1
- [8] Martin Bujnak, Zuzana Kukelova, and Tomas Pajdla. 3d reconstruction from image collections with a single known focal length. In *Computer Vision, 2009 IEEE 12th International Conference on*, pages 1803–1810. IEEE, 2009. 2, 6
- [9] Martin Byröd, Matthew A Brown, and Kalle Åström. Minimal solutions for panoramic stitching with radial distortion. In *British Machine Vision Conference (BMVC)*, 2009. 1
- [10] Federico Camposeco, Andrea Cohen, Marc Pollefeys, and Torsten Sattler. Hybrid camera pose estimation. In *Computer Vision and Pattern Recognition (CVPR)*, pages 136–144, 2018. 9
- [11] Ondřej Chum and Jiří Matas. Planar affine rectification from change of scale. In *Asian Conference on Computer Vision (ACCV)*, 2010. 4
- [12] David A. Cox, John Little, and Donal O’shea. *Using algebraic geometry*, volume 185. Springer Science & Business Media, 2006. 4
- [13] Yaqing Ding, Jian Yang, Jean Ponce, and Hui Kong. An efficient solution to the homography-based relative pose problem with a common reference direction. In *International Conference on Computer Vision (ICCV)*, 2019. 1
- [14] Andrew Fitzgibbon. Simultaneous linear estimation of multiple view geometry and lens distortion. In *Computer Vision and Pattern Recognition (CVPR)*, 2001. 1
- [15] Andreas Geiger, Philip Lenz, Christoph Stiller, and Raquel Urtasun. Vision meets robotics: The KITTI dataset. *IJRR*, 32(11):1231–1237, 2013. 9
- [16] Daniel R. Grayson and Michael E. Stillman. Macaulay2, a software system for research in algebraic geometry. Available at <http://www.math.uiuc.edu/Macaulay2/>. 4
- [17] Richard Hartley and Andrew Zisserman. *Multiple view geometry in computer vision*. Cambridge university press, 2003. 1, 3
- [18] R. I. Hartley and A. Zisserman. *Multiple View Geometry in Computer Vision*. Cambridge Univ. Press, 2nd edition, 2004. 6
- [19] D. Hook and P. R. McAree. Using sturm sequences to bracket real roots of polynomial equations. *Graphics gems*, pages 416–422, 1990. 5, 6
- [20] Hailin Jin. A three-point minimal solution for panoramic stitching with lens distortion. In *Computer Vision and Pattern Recognition (CVPR)*, 2008. 1
- [21] Alex Kendall, Matthew Grimes, and Roberto Cipolla. PoseNet: A Convolutional Network for Real-Time 6-DOF Camera Relocalization. In *ICCV*, 2015. 9
- [22] Kevin Köser. *Geometric Estimation with Local Affine Frames and Free-form Surfaces*. Shaker, 2009. 1
- [23] Zuzana Kukelova, Martin Bujnak, and Tomas Pajdla. Automatic generator of minimal problem solvers. In *European Conference on Computer Vision*, pages 302–315. Springer, 2008. 4
- [24] Zuzana Kukelova, Martin Bujnak, and Tomas Pajdla. Real-time solution to the absolute pose problem with unknown radial distortion and focal length. In *2013 IEEE International Conference on Computer Vision*, pages 2816–2823, 2013. 6, 10
- [25] Zuzana Kukelova, Jan Heller, Martin Bujnak, and Tomas Pajdla. Radial distortion homography. In *Computer Vision and Pattern Recognition (CVPR)*, 2015. 1
- [26] Zuzana Kukelova, Jan Heller, and Andrew Fitzgibbon. Efficient intersection of three quadrics and applications in computer vision. In *Computer Vision and Pattern Recognition (CVPR)*, 2016. 2
- [27] Zuzana Kukelova, Joe Kileel, Bernd Sturmfels, and Tomas Pajdla. A clever elimination strategy for efficient minimal solvers. In *Computer Vision and Pattern Recognition (CVPR)*, volume 2, page 4, 2017. 2, 4
- [28] Viktor Larsson. PoseLib - Minimal Solvers for Camera Pose Estimation. <https://github.com/vlarsson/PoseLib>, 2020. 7

- [29] Viktor Larsson, Kalle Åström, and Magnus Oskarsson. Efficient solvers for minimal problems by syzygy-based reduction. In *CVPR*, volume 2, page 4, 2017. 4
- [30] Karel Lebeda, Jiri Matas, and Ondrej Chum. Fixing the locally optimized ransac—full experimental evaluation. In *British machine vision conference*, pages 1–11. Citeseer, 2012. 9
- [31] Raul Mur-Artal, Jose Maria Martinez Montiel, and Juan D Tardos. ORB-SLAM: a versatile and accurate monocular SLAM system. *IEEE transactions on robotics*, 31(5):1147–1163, 2015. 1
- [32] Raul Mur-Artal and Juan D Tardós. ORB-SLAM2: An open-source slam system for monocular, stereo, and RGB-D cameras. *IEEE Transactions on Robotics*, 33(5):1255–1262, 2017. 1
- [33] David Nistér. An efficient solution to the five-point relative pose problem. *IEEE transactions on pattern analysis and machine intelligence*, 26(6):756–770, 2004. 2, 6, 8
- [34] Mikael Persson and Klas Nordberg. Lambda twist: An accurate fast robust perspective three point (p3p) solver. In *Proceedings of the European Conference on Computer Vision (ECCV)*, September 2018. 6
- [35] J. Philbin, O. Chum, M. Isard, J. Sivic, and A. Zisserman. Object Retrieval with Large Vocabularies and Fast Spatial Matching. In *CVPR*, 2007. 1
- [36] Robert Pless. Camera cluster in motion: motion estimation for generalized camera designs. *IEEE Robotics & Automation Magazine*, 11(4):39–44, 2004. 1
- [37] Paul-Edouard Sarlin, Cesar Cadena, Roland Siegwart, and Marcin Dymczyk. From Coarse to Fine: Robust Hierarchical Localization at Large Scale. In *The IEEE Conference on Computer Vision and Pattern Recognition (CVPR)*, 2019. 1
- [38] Torsten Sattler et al. RansacLib - A Template-based *SAC Implementation, 2019. 9
- [39] T. Sattler, B. Leibe, and L. Kobbelt. Efficient & Effective Prioritized Matching for Large-Scale Image-Based Localization. *PAMI*, 39(9):1744–1756, 2017. 1
- [40] Torsten Sattler, Qunjie Zhou, Marc Pollefeys, and Laura Leal-Taixe. Understanding the limitations of cnn-based absolute camera pose regression. In *CVPR*, 2019. 9
- [41] Olivier Saurer, Pascal Vasseur, Rémi Boutteau, Cédric Demonceaux, Marc Pollefeys, and Friedrich Fraundorfer. Homography based egomotion estimation with a common direction. *IEEE transactions on pattern analysis and machine intelligence*, 39(2):327–341, 2017. 1
- [42] Johannes L Schonberger and Jan-Michael Frahm. Structure-from-motion revisited. In *Proceedings of the IEEE Conference on Computer Vision and Pattern Recognition*, pages 4104–4113, 2016. 1
- [43] Thomas Schöps, Viktor Larsson, Marc Pollefeys, and Torsten Sattler. Why Having 10,000 Parameters in Your Camera Model Is Better Than Twelve. In *IEEE/CVF Conference on Computer Vision and Pattern Recognition (CVPR)*, 2020. 1
- [44] Noah Snavely, Steve Seitz, and Richard Szeliski. Photo tourism: exploring photo collections in 3d. In *ACM transactions on graphics (TOG)*, volume 25, pages 835–846. ACM, 2006. 1
- [45] Henrik Stewénus, D. Nistér, M. Oskarsson, and K. Åström. Solutions to minimal generalized relative pose problems. 2005. 2
- [46] Chris Sweeney, Torsten Sattler, Tobias Hollerer, Matthew Turk, and Marc Pollefeys. Optimizing the viewing graph for structure-from-motion. In *Proceedings of the IEEE International Conference on Computer Vision*, pages 801–809, 2015. 1
- [47] A. Torii, R. Arandjelović, J. Sivic, M. Okutomi, and T. Pajdla. 24/7 Place Recognition by View Synthesis. In *CVPR*, 2015. 9
- [48] A. Torii, H. Taira, J. Sivic, M. Pollefeys, M. Okutomi, T. Pajdla, and T. Sattler. Are Large-Scale 3D Models Really Necessary for Accurate Visual Localization? *IEEE Transactions on Pattern Analysis and Machine Intelligence*, pages 1–1, 2019. 9
- [49] Johanna Wald, Torsten Sattler, Stuart Golodetz, Tommaso Cavallari, and Federico Tombari. Beyond Controlled Environments: 3D Camera Re-Localization in Changing Indoor Scenes. In *European Conference on Computer Vision (ECCV)*, 2020. 2
- [50] T. Weyand and B. Leibe. Discovering Favorite Views of Popular Places with Iconoid Shift. In *ICCV*, 2011. 1
- [51] Changchang Wu. Towards linear-time incremental structure from motion. In *2013 International Conference on 3D Vision-3DV 2013*, pages 127–134. IEEE, 2013. 1
- [52] Zhengyou Zhang. A Flexible New Technique for Camera Calibration. *IEEE Transactions on Pattern Analysis and Machine Intelligence (TPAMI)*, 22:1330–1334, December 2000. 1
- [53] Enliang Zheng and Changchang Wu. Structure from motion using structure-less resection. In *International Conference on Computer Vision (ICCV)*, 2015. 2, 6, 7, 8
- [54] Enliang Zheng and Changchang Wu. Structure From Motion Using Structure-Less Resection. In *The IEEE International Conference on Computer Vision (ICCV)*, 2015. 9
- [55] Qunjie Zhou, Torsten Sattler, Marc Pollefeys, and Laura Leal-Taixe. To Learn or Not to Learn: Visual Localization from Essential Matrices. In *IEEE International Conference on Robotics and Automation (ICRA)*, 2019. 9

- [56] Qunjie Zhou, Torsten Sattler, Marc Pollefeys, and Laura Leal-Taixe. To Learn or Not to Learn: Visual Localization from Essential Matrices. *arXiv:1908.01293v1*, 2020. [9](#)

Supplementary Material

Calibrated and Partially Calibrated Semi-Generalized Homographies

Snehal Bhayani¹Torsten Sattler²
Janne Heikkilä¹Daniel Barath³
Zuzana Kukelova²Patrik Beliansky⁴¹Center for Machine Vision and Signal Analysis, University of Oulu, Finland²Faculty of Electrical Engineering, Czech Technical University in Prague³Computer Vision and Geometry group, ETH Zürich⁴Faculty of Mathematics and Physics, Charles University, Prague

1 Degeneracy for unknown focal length solvers

To obtain efficient solvers that solve only one equation in one unknown, we performed a variable substitution that was assuming that entry $g_{33} \neq 0$ (for more details, see Section 2.2 in the main paper). This substitution introduces a potential degeneracy into our solvers, *i.e.*, a degeneracy for homographies with entry $g_{33} = 0$. Our chosen coordinate system transformation allowed us to circumvent this situation for calibrated solvers. However, for the partially calibrated case this degeneracy can potentially lead to numerical instabilities of the solver when dealing with homographies with entry g_{33} close to zero. Yet, as we show next, our solvers for partially calibrated cameras are numerically stable even in situations that are very close to this degenerate case. Therefore, this degeneracy is not an issue in practical applications.

To test the numerical stability of our solvers in the close-to-degenerate case, we created various synthetic scenes by varying the magnitude of g_{33} w.r.t. normalized G and gradually bringing it closer to 0. We evaluated the performance of the proposed solvers **sH5f₂** and **sH5f₃** on these scenes. In Fig. 1, we plot the error in the estimated rotation w.r.t. the ground-truth as the magnitude of g_{33} gradually approaches 0. For this experiment we implemented **sH5f₂** using Sturm sequences [19]. For

sH5f₃, we implemented two variants, one using Sturm sequences and the other one computing eigenvalues of the companion matrix. We observe that **sH5f₂** maintains its stability even as g_{33} reaches a magnitude close to 10^{-11} . In case of the **sH5f₃** solver, our implementation based on Sturm sequences begins to experience instability w.r.t. decreasing g_{33} . In contrast, our companion matrix-based implementation remains stable. Since **sH5f₃** computes the roots of a polynomial of degree 3, there is no significant difference between the efficiency of the Sturm-based solver and the companion matrix-based solver. Therefore, we can directly use the companion matrix-based solver that is numerically stable even in close to degenerate situations.

Moreover, the proposed solvers are usually used inside RANSAC framework. Thus, after observing numerical instabilities caused by entry g_{33} being close to zero, one can always switch to a solver that is based on a different variable substitution, *i.e.*, a solver which assumes that a different entry $g_{kl} \neq 0$. Such solvers will have the same structure and will solve a similar polynomial of degree five respectively 3, as the proposed solvers.

Our assumption that entry $g_{33} \neq 0$ helped to create more efficient solvers. Yet, the main paper also considers a formulation where such an assumption is not needed. This formulation directly eliminates the mentioned degenerate configuration and it results in solving system of

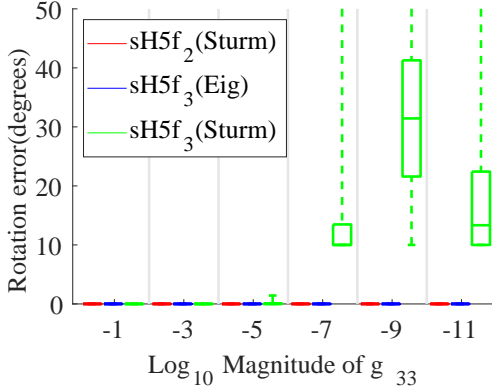


Figure 1: Error in estimated rotation(in degrees) by unknown focal length solvers, as the magnitude of g_{33} w.r.t. normalized G approaches 0. Solver **sH5f₂** was implemented with Sturm sequences while for solver **sH5f₃**, we used two implementations, one based on Sturm sequences and the other based on computing the eigenvalues of the companion matrix.

four polynomial equations in two unknowns (see Section 2.2 of the main paper). We use the automatic generator [29] to construct a Gröbner basis solver to this system of equations which performs a Gauss-Jordan elimination of a 6×12 matrix and an eigenvalue decomposition of a 6×6 matrix. Such solver is, of course, slower than the presented solver **sH5f₃** solver. However, it is still very fast and suitable for real-time applications.

2 Macaulay2 code for generating elimination ideals

The elimination ideals I_1 and I'_2 considered in Section 2.2 of our main paper have been computed using the computer algebra system Macaulay2 [16].

2.1 Unknown focal length solvers

For the unknown focal length solvers, we use the following lines of code in to generate the I_1 :

```
R = QQ[g11,g12,g13,g21,g22,g23,g31,g32,g33,
r11,r12,r13,r21,r22,r23,r31,r32,r33,
```

```
m1,m2,m3, t1,t2,t3, w ];
-- The rotation matrix
Rot = matrix {{r11,r12,r13},
              {r21,r22,r23},
              {r31,r32,r33}};
-- The plane vector
M = matrix {{m1,m2,m3}};
-- The translation vector
t = matrix{{t1},{t2},{t3}};
K = matrix {{1_R,0_R,0_R},{0_R,1_R,0_R},
            {0_R,0_R,w}};
E = matrix {{1_R,0_R,0_R},{0_R,1_R,0_R},
            {0_R,0_R,1_R}};
-- Semi-generalized homography constraint
G = Rot * K - t * M ;
```

```
I = ideal(submatrix(G,{0},{0})-g11,
          submatrix(G,{0},{1})-g12,
          submatrix(G,{0},{2})+g11,
          submatrix(G,{1},{0})-g21,
          submatrix(G,{1},{1})-g22,
          submatrix(G,{1},{2})+g21,
          submatrix(G,{2},{0})-g31,
          submatrix(G,{2},{1})-g32,
          submatrix(G,{2},{2})-g33) +
        minors(1,transpose(Rot)*Rot-E) +
        minors(1,Rot*transpose(Rot)-E) ;
```

```
-- Eliminate translation and focal length
I1 = eliminate({t1,t2,t3,w}, I) ;
```

```
-- Eliminate rotation matrix
I1 = eliminate({ r11,r12,r13,
                 r21,r22,r23,
                 r31,r32,r33}, I1) ;
```

```
betti mingens I1
```

Referring to the Section 2.2 in our main paper, we note that each variable g_{kl} , $1 \leq k, l \leq 3$ corresponds to the variable g_{kl} and m_k , $1 \leq k \leq 3$ denotes the variables m_k . The output of this code snippet shows that I_1 is generated by four polynomials, of which three are of degree 4 and one is degree 5. The following code then performs the variable substitution, where each variable g_{kl} , $1 \leq k, l \leq 3$ after the variable substitution denotes g'_{kl} and m_k , $1 \leq k \leq 3$ denotes the variables m'_k :

```
I1prime = sub(I1,
              {g11=> g33*g11, g12=> g33*g12,
```

```

g21=> g33*g21, g22=> g33*g22,
g31=> g33*g31, g32=> g33*g32,
m1=> g33*m1, m2=> g33*m2,
m3=> g33*m3 });

f0 = factor I1prime_0; f0 = f0#1#0;
f1 = factor I1prime_1; f1 = f1#1#0;
f2 = factor I1prime_2; f2 = f2#1#0;
f3 = factor I1prime_3; f3 = f3#1#0;
I1prime = ideal({f0,f1,f2,f3});
I2prime = eliminate({g33}, I1prime);
f = mingens I2prime
betty mingens I2prime

```

The output of this code are the generators of the elimination ideal I'_2 , which is in this case only one polynomial f , of degree 5 of the following form:

$$\begin{aligned}
f = & g_{11}g_{12}m_1^3 + g_{21}g_{22}m_1^3 - g_{11}^2m_1^2m_2 - \\
& g_{21}^2m_1^2m_2 + g_{11}g_{12}m_1m_2^2 + g_{21}g_{22}m_1m_2^2 - \\
& g_{11}^2m_2^3 - g_{21}^2m_2^3 + g_{11}g_{12}m_1^2m_3 + g_{21}g_{22}m_1^2m_3 + \\
& g_{31}g_{32}m_1^2m_3 - g_{11}^2m_1m_2m_3 + g_{21}^2m_1m_2m_3 - g_{21}^2m_1m_2m_3 + \\
& g_{22}^2m_1m_2m_3 - g_{31}^2m_1m_2m_3 + g_{32}^2m_1m_2m_3 - \\
& g_{11}g_{12}m_2^2m_3 - g_{21}g_{22}m_2^2m_3 - g_{31}g_{32}m_2^2m_3 - \\
& g_{32}m_1^3 + g_{31}m_1^2m_2 - g_{32}m_1m_2^2 + g_{31}m_2^3
\end{aligned}$$

(1)

2.2 Calibrated solvers

In the case of calibrated solvers, K is the identity matrix and $w = 1$. We use the following lines of code in to generate the I_1 :

```

R = QQ[g11,g12,g13,g21,g22,g23,g31,g32,g33,
r11,r12,r13,r21,r22,r23,r31,r32,r33,
m1,m2,m3, t1,t2,t3 ];
-- The rotation matrix
Rot = matrix {{r11,r12,r13},
               {r21,r22,r23},
               {r31,r32,r33}};
-- The plane vector
M = matrix {{m1,m2,m3}};
-- The translation vector
t = matrix{{t1},{t2},{t3}};
E = matrix {{1_R,0_R,0_R},{0_R,1_R,0_R},
            {0_R,0_R,1_R}};
K = E;
-- Semi-generalized homography constraint
G = Rot * K - t * M;
I = ideal(submatrix(G,{0},{0})-g11,

```

```

submatrix(G,{0},{1})-g12,
submatrix(G,{0},{2}),
submatrix(G,{1},{0})-g21,
submatrix(G,{1},{1})-g22,
submatrix(G,{1},{2}),
submatrix(G,{2},{0})-g31,
submatrix(G,{2},{1})-g32,
submatrix(G,{2},{2})-g33) +
minors(1,transpose(Rot)*Rot-E)+
minors(1,Rot*transpose(Rot)-E);

```

```

-- Eliminate translation and focal length
I1 = eliminate({t1,t2,t3}, I);
-- Eliminate rotation matrix
I1 = eliminate({ r11,r12,r13,
                  r21,r22,r23,
                  r31,r32,r33}, I1);

```

```
betty mingens I1
```

The output of this code snippet shows that in the calibrated case I_1 is generated by ten polynomials, six of which are of degree 4 and three are of degree 5 and one is of degree 6. The following code then performs the variable substitution presented in Section 2.2 of the main paper:

```

I1prime = sub(I1,
               {g11=> g33*g11, g12=> g33*g12,
g21=> g33*g21, g22=> g33*g22,
g31=> g33*g31, g32=> g33*g32,
m1=> g33*m1, m2=> g33*m2,
m3=> g33*m3 });

f0 = factor I1prime_0; f0 = f0#1#0;
f1 = factor I1prime_1; f1 = f1#1#0;
f2 = factor I1prime_2; f2 = f2#1#0;
f3 = factor I1prime_3; f3 = f3#1#0;
f4 = factor I1prime_4; f4 = f4#1#0;
f5 = factor I1prime_5; f5 = f5#1#0;
f6 = factor I1prime_6; f6 = f6#1#0;
f7 = factor I1prime_7; f7 = f7#1#0;
f8 = factor I1prime_8; f8 = f8#1#0;
f9 = factor I1prime_9; f9 = f9#0#0;
I1prime = ideal({f0,f1,f2,f3,f4,f5,f6,f7,f8,f9});
I2prime = eliminate({g33}, I1prime);

f = mingens I2prime
betty mingens I2prime

```

The output of this code are generators of the elimination ideal I'_2 , which is in this case generated by a set of five polynomials, each of which is of degree 5. While we can choose one of these polynomials for generating a solver, we note that the stability of the solver would be similar irrespective of which one of these polynomials is used. For our proposed solvers, **sH5₃** and **sH5₂** we used the first polynomial f_1 ,

$$f_1 = g_{12}^2 m_1 m_2 m_3 + g_{22}^2 m_1 m_2 m_3 + g_{32}^2 m_1 m_2 m_3 - g_{11} g_{12} m_2^2 m_3 - g_{21} g_{22} m_2^2 m_3 - g_{31} g_{32} m_2^2 m_3 - g_{11} g_{12} m_3^3 - g_{21} g_{22} m_3^3 - g_{31} g_{32} m_3^3 - g_{32} m_1 m_2^2 + g_{31} m_2^3 + g_{32} m_1 m_2^2 + g_{31} m_2 m_2^3 - m_1 m_2 m_3. \quad (2)$$

3 Graphs for synthetic experiments

For our synthetic experiments, we computed relative error in pose with respect to its ground-truth value, $t_\delta = \frac{\|\mathbf{t} - \mathbf{t}_{GT}\|}{\|\mathbf{t}_{GT}\|}$, and the relative error in focal length with respect to its ground truth value $f_\delta = \frac{|f - f_{GT}|}{|f_{GT}|}$. Here \mathbf{t}_{GT} and f_{GT} respectively denote the ground-truth value of pose and focal length. These errors are plotted in figures 2 and 3 which demonstrate respectively, the performance of the unknown focal length solvers and calibrated solvers in terms of numerical stability, solver performance in presence of image noise, solver performance in the presence of close-to-planar scenes and stability in the presence of forward motion and image noise. For both of the cases, we observe that our proposed solvers have comparable numerical stability to the state-of-the-art solvers in estimating pose and focal length (for partially calibrated solvers).

4 Details on the Localization Experiments

As stated in Sec. 3.3 of the main paper (“Localization Experiment”), this section provides additional details on the localization experiments presented in the paper.

All solvers (**sH5₂**, **sH5₃**, **E₅₊₁**, and **E₄₊₂**) are integrated into the LO-RANSAC [30] implementation provided by [38] and we run RANSAC for at least 100 and

at most 10,000 iterations. We modified the RANSAC implementation to skip the non-minimal solver inside the local optimization (LO) stage. We instead directly perform least-squares refinement of the estimated model using a random subset of the inliers of the best model found so far by one of the solvers. After LO-RANSAC, the estimated model is refined on all of its inliers using the same non-linear optimization approach. The non-linear optimization is implemented using the Ceres library [1].

For inlier counting, we either measure the reprojection error via the estimated semi-generalized homography or triangulate a 3D point given the estimated pose of the pinhole camera with respect to the generalized camera and measure the reprojection error of that point. We use the same threshold (about 10 pixels, which corresponds to about 1% of the image diagonal of the images as we use images of size 800×450 pixels for our experiments). For the **E₅₊₁** and **E₄₊₂**, we use the latter. For our two solvers (**sH5₂**, **sH5₃**), we first extract the pose of the pinhole camera with respect to the generalized camera from the estimated semi-generalized homography. We then measure both types of reprojection errors and report the minimal one for inlier counting. This enables us to also count inliers on non-planar structures. For a given inlier match, we minimize the corresponding reprojection error (either based on the semi-generalized homography or the triangulated 3D point, depending on which one is smaller) during non-linear refinement. Inside RANSAC, we randomly sample from all input matches. However, not all combinations of matches is a valid input for each solver, e.g., the **E₄₊₂** solver requires four matches from the first and two matches from the second camera in the generalized camera. In the case that the draw sample does not fit the solver, we skip running the minimal solver in this iteration. Since all solvers have this problem, we consider the experiments fair, especially since we did not observe that RANSAC needed the maximum number of iterations for any of the test images.

References

- [1] Sameer Agarwal, Keir Mierle, and Others. Ceres solver. <http://ceres-solver.org>. 4
- [2] Daniel Barath. Five-point fundamental matrix estimation for uncalibrated cameras. In *Proceedings of the IEEE*

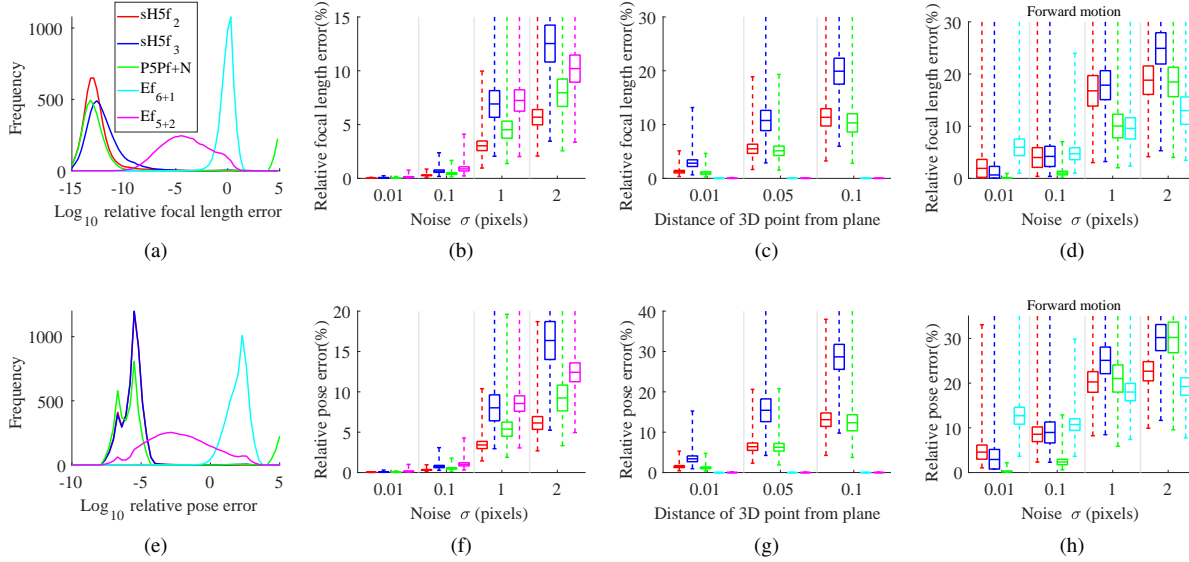


Figure 2: Solvers for partially calibrated cameras, Top: Ground-truth error in focal length, Bottom: Ground-truth error in pose, for (a,e) Numerical stability, (b,f) Performance in the presence of image noise, (c,g) Close-to-planar scenes, and (d,h) Forward motion in the presence of image noise.

- Conference on Computer Vision and Pattern Recognition*, pages 235–243, 2018.
- [3] Daniel Barath and Levente Hajder. A theory of point-wise homography estimation. *Pattern Recognition Letters*, 94:7–14, 2017.
 - [4] Daniel Barath and Zuzana Kukelova. Homography from two orientation-and scale-covariant features. In *Proceedings of the IEEE International Conference on Computer Vision*, pages 1091–1099, 2019.
 - [5] Daniel Barath and Jiří Matas. Graph-cut RANSAC. In *Computer Vision and Pattern Recognition (CVPR)*, 2018.
 - [6] Eric Brachmann and Carsten Rother. Expert sample consensus applied to camera re-localization. In *ICCV*, 2019.
 - [7] Matthew Brown, Richard I Hartley, and David Nistér. Minimal solutions for panoramic stitching. In *2007 IEEE Conference on Computer Vision and Pattern Recognition*, pages 1–8. IEEE, 2007.
 - [8] Martin Bujnak, Zuzana Kukelova, and Tomas Pajdla. 3d reconstruction from image collections with a single known focal length. In *Computer Vision, 2009 IEEE 12th International Conference on*, pages 1803–1810. IEEE, 2009.
 - [9] Martin Byröd, Matthew A Brown, and Kalle Åström. Minimal solutions for panoramic stitching with radial distortion. In *British Machine Vision Conference (BMVC)*, 2009.
 - [10] Federico Camposeco, Andrea Cohen, Marc Pollefeys, and Torsten Sattler. Hybrid camera pose estimation. In *Computer Vision and Pattern Recognition (CVPR)*, pages 136–144, 2018.
 - [11] Ondřej Chum and Jiří Matas. Planar affine rectification from change of scale. In *Asian Conference on Computer Vision (ACCV)*, 2010.
 - [12] David A. Cox, John Little, and Donal O’shea. *Using algebraic geometry*, volume 185. Springer Science & Business Media, 2006.
 - [13] Yaqing Ding, Jian Yang, Jean Ponce, and Hui Kong. An efficient solution to the homography-based relative pose problem with a common reference direction. In *International Conference on Computer Vision (ICCV)*, 2019.
 - [14] Andrew Fitzgibbon. Simultaneous linear estimation of multiple view geometry and lens distortion. In *Computer Vision and Pattern Recognition (CVPR)*, 2001.
 - [15] Andreas Geiger, Philip Lenz, Christoph Stiller, and Raquel Urtasun. Vision meets robotics: The KITTI dataset. *IJRR*, 32(11):1231–1237, 2013.
 - [16] Daniel R. Grayson and Michael E. Stillman. Macaulay2, a software system for research in algebraic geometry.

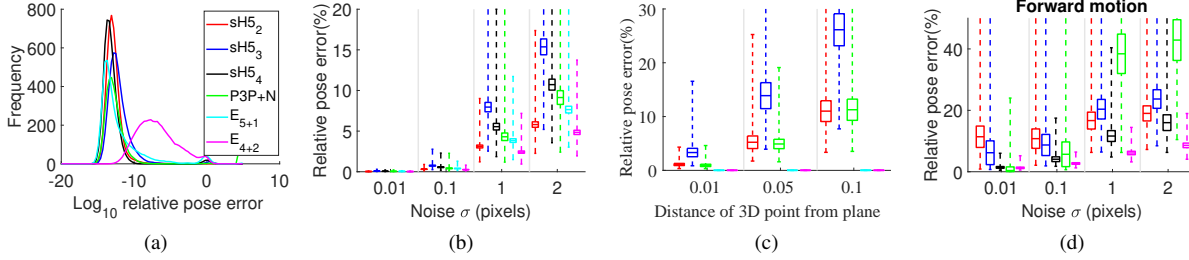


Figure 3: Ground-truth error in pose for solvers for calibrated cameras, for (a) Numerical stability, (b) Performance in the presence of image noise, (c) Close-to-planar scenes and (d) Forward motion in the presence of image noise.

- try. Available at <http://www.math.uiuc.edu/Macaulay2/>. 2
- [17] Richard Hartley and Andrew Zisserman. *Multiple view geometry in computer vision*. Cambridge university press, 2003.
- [18] R. I. Hartley and A. Zisserman. *Multiple View Geometry in Computer Vision*. Cambridge Univ. Press, 2nd edition, 2004.
- [19] D. Hook and P. R. McAree. Using sturm sequences to bracket real roots of polynomial equations. *Graphics gems*, pages 416–422, 1990. 1
- [20] Hailin Jin. A three-point minimal solution for panoramic stitching with lens distortion. In *Computer Vision and Pattern Recognition (CVPR)*, 2008.
- [21] Alex Kendall, Matthew Grimes, and Roberto Cipolla. PoseNet: A Convolutional Network for Real-Time 6-DOF Camera Relocalization. In *ICCV*, 2015.
- [22] Kevin Köser. *Geometric Estimation with Local Affine Frames and Free-form Surfaces*. Shaker, 2009.
- [23] Zuzana Kukelova, Martin Bujnak, and Tomas Pajdla. Automatic generator of minimal problem solvers. In *European Conference on Computer Vision*, pages 302–315. Springer, 2008.
- [24] Zuzana Kukelova, Martin Bujnak, and Tomas Pajdla. Real-time solution to the absolute pose problem with unknown radial distortion and focal length. In *2013 IEEE International Conference on Computer Vision*, pages 2816–2823, 2013.
- [25] Zuzana Kukelova, Jan Heller, Martin Bujnak, and Tomas Pajdla. Radial distortion homography. In *Computer Vision and Pattern Recognition (CVPR)*, 2015.
- [26] Zuzana Kukelova, Jan Heller, and Andrew Fitzgibbon. Efficient intersection of three quadrics and applications in computer vision. In *Computer Vision and Pattern Recognition (CVPR)*, 2016.
- [27] Zuzana Kukelova, Joe Kileel, Bernd Sturmfels, and Tomas Pajdla. A clever elimination strategy for efficient minimal solvers. In *Computer Vision and Pattern Recognition (CVPR)*, volume 2, page 4, 2017.
- [28] Viktor Larsson. PoseLib - Minimal Solvers for Camera Pose Estimation. <https://github.com/vlarsson/PoseLib>, 2020.
- [29] Viktor Larsson, Kalle Åström, and Magnus Oskarsson. Efficient solvers for minimal problems by syzygy-based reduction. In *CVPR*, volume 2, page 4, 2017. 2
- [30] Karel Lebeda, Jiri Matas, and Ondrej Chum. Fixing the locally optimized ransac—full experimental evaluation. In *British machine vision conference*, pages 1–11. Citeseer, 2012. 4
- [31] Raul Mur-Artal, Jose Maria Martinez Montiel, and Juan D Tardos. ORB-SLAM: a versatile and accurate monocular SLAM system. *IEEE transactions on robotics*, 31(5):1147–1163, 2015.
- [32] Raul Mur-Artal and Juan D Tardós. ORB-SLAM2: An open-source slam system for monocular, stereo, and RGB-D cameras. *IEEE Transactions on Robotics*, 33(5):1255–1262, 2017.
- [33] David Nistér. An efficient solution to the five-point relative pose problem. *IEEE transactions on pattern analysis and machine intelligence*, 26(6):756–770, 2004.
- [34] Mikael Persson and Klas Nordberg. Lambda twist: An accurate fast robust perspective three point (p3p) solver. In *Proceedings of the European Conference on Computer Vision (ECCV)*, September 2018.
- [35] J. Philbin, O. Chum, M. Isard, J. Sivic, and A. Zisserman. Object Retrieval with Large Vocabularies and Fast Spatial Matching. In *CVPR*, 2007.
- [36] Robert Pless. Camera cluster in motion: motion estimation for generalized camera designs. *IEEE Robotics & Automation Magazine*, 11(4):39–44, 2004.

- [37] Paul-Edouard Sarlin, Cesar Cadena, Roland Siegwart, and Marcin Dymczyk. From Coarse to Fine: Robust Hierarchical Localization at Large Scale. In *The IEEE Conference on Computer Vision and Pattern Recognition (CVPR)*, 2019.
- [38] Torsten Sattler et al. RansacLib - A Template-based *SAC Implementation, 2019. 4
- [39] T. Sattler, B. Leibe, and L. Kobbelt. Efficient & Effective Prioritized Matching for Large-Scale Image-Based Localization. *PAMI*, 39(9):1744–1756, 2017.
- [40] Torsten Sattler, Qunjie Zhou, Marc Pollefeys, and Laura Leal-Taixe. Understanding the limitations of cnn-based absolute camera pose regression. In *CVPR*, 2019.
- [41] Olivier Saurer, Pascal Vasseur, Rémi Boutheau, Cédric Demonceaux, Marc Pollefeys, and Friedrich Fraundorfer. Homography based egomotion estimation with a common direction. *IEEE transactions on pattern analysis and machine intelligence*, 39(2):327–341, 2017.
- [42] Johannes L Schonberger and Jan-Michael Frahm. Structure-from-motion revisited. In *Proceedings of the IEEE Conference on Computer Vision and Pattern Recognition*, pages 4104–4113, 2016.
- [43] Thomas Schöps, Viktor Larsson, Marc Pollefeys, and Torsten Sattler. Why Having 10,000 Parameters in Your Camera Model Is Better Than Twelve. In *IEEE/CVF Conference on Computer Vision and Pattern Recognition (CVPR)*, 2020.
- [44] Noah Snavely, Steve Seitz, and Richard Szeliski. Photo tourism: exploring photo collections in 3d. In *ACM transactions on graphics (TOG)*, volume 25, pages 835–846. ACM, 2006.
- [45] Henrik Stewénius, D. Nistér, M. Oskarsson, and K. Åström. Solutions to minimal generalized relative pose problems. 2005.
- [46] Chris Sweeney, Torsten Sattler, Tobias Hollerer, Matthew Turk, and Marc Pollefeys. Optimizing the viewing graph for structure-from-motion. In *Proceedings of the IEEE International Conference on Computer Vision*, pages 801–809, 2015.
- [47] A. Torii, R. Arandjelović, J. Sivic, M. Okutomi, and T. Pajdla. 24/7 Place Recognition by View Synthesis. In *CVPR*, 2015.
- [48] A. Torii, H. Taira, J. Sivic, M. Pollefeys, M. Okutomi, T. Pajdla, and T. Sattler. Are Large-Scale 3D Models Really Necessary for Accurate Visual Localization? *IEEE Transactions on Pattern Analysis and Machine Intelligence*, pages 1–1, 2019.
- [49] Johanna Wald, Torsten Sattler, Stuart Golodetz, Tommaso Cavallari, and Federico Tombari. Beyond Controlled Environments: 3D Camera Re-Localization in Changing Indoor Scenes. In *European Conference on Computer Vision (ECCV)*, 2020.
- [50] T. Weyand and B. Leibe. Discovering Favorite Views of Popular Places with Iconoid Shift. In *ICCV*, 2011.
- [51] Changchang Wu. Towards linear-time incremental structure from motion. In *2013 International Conference on 3D Vision-3DV 2013*, pages 127–134. IEEE, 2013.
- [52] Zhengyou Zhang. A Flexible New Technique for Camera Calibration. *IEEE Transactions on Pattern Analysis and Machine Intelligence (TPAMI)*, 22:1330–1334, December 2000.
- [53] Enliang Zheng and Changchang Wu. Structure from motion using structure-less resection. In *International Conference on Computer Vision (ICCV)*, 2015.
- [54] Enliang Zheng and Changchang Wu. Structure From Motion Using Structure-Less Resection. In *The IEEE International Conference on Computer Vision (ICCV)*, 2015.
- [55] Qunjie Zhou, Torsten Sattler, Marc Pollefeys, and Laura Leal-Taixe. To Learn or Not to Learn: Visual Localization from Essential Matrices. In *IEEE International Conference on Robotics and Automation (ICRA)*, 2019.
- [56] Qunjie Zhou, Torsten Sattler, Marc Pollefeys, and Laura Leal-Taixe. To Learn or Not to Learn: Visual Localization from Essential Matrices. *arXiv:1908.01293v1*, 2020.